# UC Irvine
## UC Irvine Previously Published Works


### Title
Distinct Functions of Human Cohesin-SA1 and Cohesin-SA2 in Double-Strand Break Repair


### Permalink
https://escholarship.org/uc/item/3t12c4m2



### Journal
Molecular and Cellular Biology, 34(4)

### ISSN
0270-7306



### Authors
Kong, Xiangduo
Ball, Alexander R
Pham, Hoang Xuan
et al.



### Publication Date
2014-02-01

### DOI
10.1128/mcb.01503-13

Peer reviewed



eScholarship.org Powered by the California Digital Library
University of California

MCB
Journals.ASM.org

# Distinct Functions of Human Cohesin-SA1 and Cohesin-SA2 in Double-Strand Break Repair

**Xiangduo Kong,[a] Alexander R. Ball, Jr.,[a] Hoang Xuan Pham,[a] Weihua Zeng,[a]* Hsiao-Yuan Chen,[a] John A. Schmiesing,[a] Jong-Soo Kim,[a]* Michael Berns,[b,c] Kyoko Yokomori[a]**

Department of Biological Chemistry, School of Medicine, University of California, Irvine, California, USA[a]; Beckman Laser Institute[b] and Department of Biomedical Engineering, Samueli School of Engineering,[c] University of California, Irvine, California, USA

**Cohesin is an essential multiprotein complex that mediates sister chromatid cohesion critical for proper segregation of chromosomes during cell division. Cohesin is also involved in DNA double-strand break (DSB) repair. In mammalian cells, cohesin is involved in both DSB repair and the damage checkpoint response, although the relationship between these two functions is unclear. Two cohesins differing by one subunit (SA1 or SA2) are present in somatic cells, but their functional specificities with regard to DNA repair remain enigmatic. We found that cohesin-SA2 is the main complex corecruited with the cohesin-loading factor NIPBL to DNA damage sites in an S/$G_2$-phase-specific manner. Replacing the diverged C-terminal region of SA1 with the corresponding region of SA2 confers this activity on SA1. Depletion of SA2 but not SA1 decreased sister chromatid homologous recombination repair and affected repair pathway choice, indicating that DNA repair activity is specifically associated with cohesin recruited to damage sites. In contrast, both cohesin complexes function in the intra-S checkpoint, indicating that cell cycle-specific damage site accumulation is not a prerequisite for cohesin's intra-S checkpoint function. Our findings reveal the unique ways in which cohesin-SA1 and cohesin-SA2 participate in the DNA damage response, coordinately protecting genome integrity in human cells.**

DNA double-strand breaks (DSBs) are deleterious to genome integrity and can result in chromosomal breakage or translocations and cell death. The two major mechanisms to repair DSBs are the error-prone nonhomologous end joining (NHEJ) and the error-free homologous-recombination (HR) pathways, which involve distinct sets of repair proteins (1). While NHEJ operates throughout the cell cycle, HR utilizes an intact sister chromatid as a repair template and thus is restricted to S/$G_2$ phase in mammalian cells. Although the two pathways complement one another, the error-free HR pathway is particularly important for accurate damage repair. DSBs also evoke DNA damage checkpoint responses that are mediated by ATM (and the related ATR) (1–3). The $G_1$/S and $G_2$/M checkpoints, which inhibit cell cycle progression, and the intra-S checkpoint, which inhibits DNA replication, together provide adequate time for DNA repair. Both the checkpoint and the repair functions coordinately maintain genome integrity and stability.

The primary function of cohesin is to mediate genome-wide sister chromatid cohesion in a cell cycle-regulated manner to ensure proper segregation of chromosomes in mitosis (4–8). Cohesin contains two SMC proteins (SMC1 and SMC3) and the two non-SMC subunits Rad21 (Scc1) and SA (Scc3 or STAG). Whereas a single Scc3 is present in yeast, two SA proteins, SA1 and SA2, are found in higher eukaryotes that form two distinct cohesin complexes in somatic cells: cohesin-SA1 and cohesin-SA2 (9, 10). Both cohesin-SA1 and cohesin-SA2 contribute to genome-wide sister chromatid cohesion, although SA1 is particularly important for telomeric sister chromatid cohesion in mammalian cells (9, 11–13). Cohesin requires additional factors for its function, including NIPBL (Scc2 or delangin) and its partner MAU-2 (Scc4) for cohesin loading onto chromatin in telophase in mammalian cells (14–17).

Cohesin also plays a role in DSB repair (18). Using green laser microirradiation, we demonstrated that human cohesin is recruited to DNA damage sites in an S/$G_2$-specific and Mre11-Rad50-dependent manner (19). Consistent with the cell cycle-specific damage site recruitment, cohesin is involved in sister chromatid HR but not NHEJ in human cells (20). Similar Mre11-dependent accumulation of cohesin at endonuclease-induced DSB sites was required for postreplicative DNA repair in *Saccharomyces cerevisiae* (21, 22). It was found that the cohesion function of yeast cohesin is activated genome-wide in response to damage (23, 24). Although not explicitly proven in human cells, the model asserts that cohesin is recruited to the damage sites and facilitates sister chromatid HR by mediating local cohesion between a damaged chromatid and its intact sister template (19).

Cohesin is also involved in damage checkpoint responses in mammalian cells (25–27). SMC1 and SMC3 are phosphorylated by ATM/ATR in response to DNA damage, which is critical for the intra-S checkpoint (25, 27, 28). Cohesin's role in checkpoint control has not been observed in yeast (29), suggesting species-specific differences of cohesin regulation and function in the DNA damage response. Interestingly, although cohesin is recruited to damage sites only in the S/$G_2$ phase (19), cohesin is phosphory-

**Received** 14 November 2013 **Accepted** 2 December 2013

**Published ahead of print** 9 December 2013

Address correspondence to Kyoko Yokomori, kyokomor@uci.edu.

* Present address: Weihua Zeng, Department of Developmental and Cell Biology, School of Biological Science, University of California, Irvine, California, USA; Jong-Soo Kim, Chungbuk National University, Research Institute of Veterinary Medicine, Heungdeok-gu, Cheongju Chungbuk, Republic of Korea.

Supplemental material for this article may be found at http://dx.doi.org/10.1128/MCB.01503-13.

Copyright © 2014, American Society for Microbiology. All Rights Reserved.

doi:10.1128/MCB.01503-13

lated by ATM and is required for efficient Chk2 activation even in $G_1$ phase (26, 30). These observations suggest that cohesin's roles in the checkpoint response and in DNA repair may be separate. At present, however, both functions are assumed to be mediated by cohesin at damage sites (26, 31, 32), and no clear distinction has been made between cohesins involved in HR repair and checkpoint control. We characterized here cohesin recruitment to damage sites in detail and obtained evidence that the repair and intra-S checkpoint functions are separate, with the former function primarily mediated by cohesin-SA2 selectively recruited to damage sites in human cells.

## MATERIALS AND METHODS

**Cell lines, clones, and cell synchronization.** HeLa cells were cultured as described previously (19). The HeLa hSMC1-GFP stable cell line was characterized and described previously (33). The pIRESneo3 (BD Biosciences Clontech) plasmids encoding green fluorescent protein (GFP)-tagged full-length SA1 (amino acids [aa] 1 to 1258) and SA2 (SA2b; aa 1 to 1231), deletion mutants (SA1N (aa 1 to 266), SA1NM (aa 1 to 1027), SA1C (aa 1028 to 1258), SA2N (aa 1 to 263), SA2NM (aa 1 to 1023), SA2C (aa 1024 to 1231), SA2ΔNLS2NLS3 missing the last two nuclear localization signals (NLSs; aa 1 to 1128), SA2ΔNLS3 missing the last NLS (aa 1 to 1169), NLS alanine substitution mutants, and chimeric mutants (SA1NSA2MC, SA2NSA1MC, and SA1NMSA2C) were transfected into HeLa cells using PolyFect (Qiagen). To make stable cell lines, transfected cells were selected by resistance to 0.5 mg of G418/ml. HeLa cells were synchronized to S phase by double thymidine block (see Fig. S1 in the supplemental material) (34). For $G_1$ cells, mitotic cells were marked on gridded coverslips. After 3 h, the daughter cells were subjected to DNA damage. Cells were immunostained for cyclin B1 or Rad51 to further confirm the cell cycle stage.

**Laser microirradiation.** Laser damage induction and image analysis were carried out essentially as described previously (35, 36). In brief, 532 nm of the second harmonic of a pulsed Nd:YAG laser beam (~2 to 3 μJ/pulse energy after objective; ~4- to 6-ns pulse duration; 7.5 Hz; Quantronix-Continuum Lasers, La Mesa, CA) was focused through a 100× Ph3 UPlanFI oil objective lens (numerical aperture [NA], 1.3; Olympus) on a microscope (model IX81; Olympus). Near-infrared (NIR) femtosecond laser irradiation was carried out using a Zeiss LSM 510 META multiphoton-equipped (3.0-W 170-fs coherent tunable Chameleon Ultra-NIR laser) confocal microscope. The Chameleon NIR beam was tuned to 780 nm, where the software bleach function was used to target linear tracts inside the cell nuclei for exposure to single laser scans (6.3 μs pixel dwell time, $\sim 7.0 \times 10^{11}$ W/cm$^2$) through the 100× objective lens (1.4 NA Zeiss Plan APO). Since similar results were obtained with the green and NIR lasers, these two laser systems were used interchangeably in the present study. Five to seven cells were damaged in one plate, and three to four plates were subjected to laser damage in each experiment.

**I-PpoI-mediated DSB induction.** Cells were transfected with the ER-I-PpoI expression plasmid and, 24 h later, 4-hydroxy-tamoxifen (4-OHT; Sigma) was added to a final concentration of 1 μM for 10 h to induce the nuclear localization of ER-I-PpoI as described previously (37).

**Gamma irradiation.** Gamma irradiation was performed using a cesium-137 source irradiator (J. L. Shepherd Mark I; dose rate, 2.02 Gy/min). Cell dishes were kept rotating on the turntable inside the irradiator during the irradiation procedure.

**Antibodies.** Antibodies specific for hSMC1 and Rad21 were previously described (34). Rabbit polyclonal antibody against the NIPBL protein was raised against a bacterially expressed recombinant polypeptide corresponding to an N-terminal fragment of NIPBL (aa 1 to 380). Mouse monoclonal antibodies specific for Mre11 and Rad50 (GeneTex, Inc.), GFP (Clontech Laboratories, Inc.), cyclin B1 (Santa Cruz Biotechnology, Inc.), γH2AX and Rad21 (Upstate Biotechnologies), phospho-SMC1 (Ser957; Cell Signaling), and β-tubulin (Sigma), rabbit polyclonal antibodies specific for GFP (Clontech Laboratories, Inc.), γH2AX (Millipore), phospho-Chk2 (Thr68; Cell Signaling), and Rad51 (Santa Cruz Biotechnology, Inc.), and goat polyclonal antibodies specific for SA1 and SA2 (Bethyl Laboratories, Inc.) were also used.

**Immunofluorescent staining and image analysis.** At different time points after damage induction, cells were fixed in 4% paraformaldehyde (15 min at 4°C), permeabilized in 0.5% Triton X-100 for five min (4°C), and stained with antibodies. In some cases, cells were fixed with 100% methanol (−20°C) without detergent extraction to reveal cytoplasmic localization of cohesin subunits. The staining procedure was described previously (19). Fluorescent images were captured through a 100× Ph3 UPlanFI oil objective lens (NA, 1.3; Olympus) on a model IX81 Olympus microscope with a charge-coupled device camera. The immunofluorescent signals at damage sites were measured using MicroSuite FIVE Imaging Software (Olympus). Recruitment of GFP-fusion proteins to damage sites was observed by live-cell confocal scanning with the 488-nm CW argon laser on the same Zeiss META platform. Experiments were repeated at least three times and consistent results were obtained. Fluorescent measurement of the recruitment of GFP-tagged proteins to damage sites was performed by live-cell confocal scanning with the 488-nm CW argon laser on the Zeiss LSM 510 META platform. The signals were measured with the LSM510 software (version 4.0).

**Co-IP and Western blot analysis.** Nuclear extract preparation and coimmunoprecipitation (co-IP) were performed as described previously (38, 39). For the co-IP experiments in Fig. S5 in the supplemental material, the cells were lysed in TNE buffer (10 mM Tris [pH 7.8], 1% Nonidet P-40, 0.15 M NaCl, 1 mM EDTA, and protease inhibitor cocktail [Sigma]) on ice for 1 h as described previously (11). Immunoprecipitated proteins on beads were washed first with low salt followed by 1 M salt, and then eluted with 2 M guanidine-HCl. Alternatively, four washes with 0.4 M salt were used. Eluted fractions were precipitated with trichloroacetic acid and separated by SDS-PAGE, followed by Western blotting.

**siRNA depletion.** HeLa cells were transfected twice (except for Rad21 small interfering RNA [siRNA], which was once) 24 h apart with siRNAs at a final concentration of 5 nM using HiPerFect transfection reagent according to the manufacturer's instructions (Qiagen). siRNAs directed against hSMC1 (5′-CACCATCACACTTTAATTCCA-3′), hRad21 (5′-ATCGATGAGCCCATTATTGAA-3′), SA1 (5′-CACGTAGAATCAGATGTTCTA-3′), and SA2 (5′-TCGGTGGTAGATGATTGGATA-3′) as described previously (40) and NIPBL (5′-CTAGCTGACTCTGACAATAAA-3′) or a negative-control siRNA (Qiagen) were used. Cells were harvested for Western blot analyses or subjected to laser microirradiation, approximately 24 h after the final transfection.

**Sister chromatid exchange (SCE) assays.** HeLa cells were transfected with the indicated siRNA oligonucleotides and synchronized by a double thymidine block. After release from the first thymidine block, cells were incubated in the presence of 10 μM bromodeoxyuridine to achieve preferential labeling of sister chromatids. After the second thymidine block, mitomycin C was added to the culture at a final concentration of 20 ng/ml. Seven hours later, colcemid was added at a final concentration of 0.05 μg/ml to accumulate mitotic cells. Harvested cells were then incubated in 75 mM KCl for 15 min at room temperature and then fixed with 3:1 (vol/vol) methanol-glacial acetic acid. Sister chromatid differentiation was performed as described previously (41). Experiments were repeated three times, and a total of 200 chromosomes were examined.

**NHEJ assay.** Cells were twice transfected with control, SA1, or SA2 siRNA. At 48 h after initial transfection, the cells were transfected with an mCherry expression plasmid, together with an EGFP-pIRES plasmid linearized with EcoRI, uncoupling the transcriptional promoter from the enhanced GFP (EGFP) open reading frame. The end-joining frequency was determined by calculating the percentage of EGFP-positive cells in the mCherry-positive cells by fluorescence-activated cell sorting (FACS) at 24 h after transfection as described previously (42). Approximately 15 to 20% of mCherry-positive-control siRNA-treated cells were EGFP posi-

tive. Experiments were repeated three times, and a total of $6 \times 10^5$ cells were examined.

**$G_2$/M checkpoint assay.** Synchronized HeLa cells were transfected with siRNAs and irradiated (4 Gy) in $G_2$ phase after release from the second block, with or without caffeine treatment. The cell cycle stage was confirmed by FACS analysis of DNA content of siRNA-treated cells (see below), as well as the morphology of the cells under the microscope. Nocodazole was then added to a final concentration of 0.04 μg/ml to block cells in mitotic phase. The mitotic index was determined by counting the mitotic cells among 5,000 total cells in three separate experiments.

**Radioresistant DNA synthesis (RDS) assay.** IR-induced inhibition of DNA synthesis was measured as previously described (43). At 6 h after the second transfection with the indicated siRNAs, cells were labeled for 24 h with 10 nCi of [$^{14}$C]thymidine/ml. The third siRNA transfection was performed after 18 h of the [$^{14}$C]thymidine incubation. The cells were then seeded at a density of $3 \times 10^5$ cells/35-mm dish and then incubated for another 24 h in nonradioactive medium before treatment with 0 or 10 Gy of gamma irradiation. At 30 min after irradiation (10 Gy), 1.0 μCi of [$^3$H]thymidine/ml was added to the medium for 30 min to allow cell labeling. The cells were collected and transferred to Whatman filters and fixed sequentially with 70% methanol, followed by 95% methanol. Radioactivity was measured in a liquid scintillation counter. Radioresistant DNA synthesis was assessed by taking the ratios of [$^3$H]/[$^{14}$C] and was normalized against the same siRNA-treated undamaged cells.

**Cell survival assay.** Just prior to the second thymidine block, synchronized cells (transfected with the indicated siRNAs) were seeded at a density of 1,000 cells/10-cm plate. At 6 h after release from the second block, the cells were exposed to 5 Gy of gamma irradiation. Two weeks later colonies were fixed with 100% ethanol and stained with 0.006% crystal violet. Colonies with 50 or more cells were counted.

**FACS analysis of DNA content.** Cells were treated with siRNA and synchronized by a double-thymidine block. After release from the second thymidine block, cells were harvested at different time points and were fixed with 70% ethanol at −20°C for at least 30 min. The cells were then washed with phosphate-buffered saline and stained with 10 μg of propidium iodide/ml in the presence of 5 μg of RNase A/ml (34). FACS analysis was performed using a Becton Dickinson FACSCalibur cell analyzer.

**ChIP analysis of I-PpoI sites.** Chromatin immunoprecipitation (ChIP) assays were carried out according to the protocol described (44, 45) with modifications. Briefly, HeLa cells were transfected twice (24 h apart) with siRNAs against SA1, SA2, or a negative-control siRNA. At 8 h after the second siRNA transfection, the cells were synchronized with a double thymidine block. The cells were mock transfected, which allowed them to serve as undamaged control cells, or transfected with a plasmid encoding I-PpoI fused to the estrogen receptor (ER-I-PpoI) 2 h after release from the first thymidine block. At 24 h after ER-I-PpoI or mock transfection, 1 mM 4-OHT was added to the medium for 4 h to induce the nuclear translocation of ER-I-PpoI and DNA cleavage. The cells were harvested for ChIP experiments using anti-Rad21 antibody (45) or preimmune IgG. ChIP signals were analyzed by quantitative PCR (qPCR) with primers specific for the I-PpoI cut site (44) and the known cohesin binding site in the H19 gene region (46). The ChIP qPCR signals were normalized by the subtraction of the preimmune IgG ChIP signal and further divided by the input. The data were expressed relative to the signal obtained from cells treated with the corresponding siRNA without I-PpoI plasmid transfection.

## RESULTS

**S/$G_2$-specific accumulation of cohesin at DSB damage sites.** We previously determined that the green and near-infrared (NIR) laser systems are suitable for faithfully recapitulating damage responses elicited by conventional DSB-inducing agents (35, 47). We demonstrated that the damage site recruitment of cohesin can be studied using these systems (19, 44). We showed that despite the presence of cohesin in the nucleus, recruitment of cohesin subunit hSMC1 to laser-induced damage sites does not occur in the $G_1$ phase in human cells (19). However, a recent study using ChIP analysis of endonuclease-induced DSB sites reported that the recruitment of Rad21 (Scc1) is not cell cycle specific (48). Thus, we decided to reexamine cohesin recruitment to damage sites at different cell cycle stages. We observed that Rad21 and HR repair factor Rad51 clustering to laser-induced damage sites failed to occur in newly divided $G_1$ cells, a finding consistent with our previous study (19) (Fig. 1A and B). In contrast, Rad21 recruitment to damage sites was robustly observed in S/$G_2$ cells in parallel with Rad51 (Fig. 1A and B). The stably expressed GFP-tagged hSMC1 (hSMC1-GFP) also failed to accumulate at damage sites in $G_1$ phase (see Fig. S2A in the supplemental material). Proper subcellular localization and incorporation of the recombinant hSMC1-GFP into the cohesin complex was confirmed previously (33).

To eliminate the possibility that the observed cell cycle-regulated cohesin clustering at damage sites is a laser-induced damage-specific phenomenon, we examined cohesin accumulation at I-PpoI endonuclease-induced DSB sites (Fig. 1C). I-PpoI creates site-specific DSBs in the ribosomal DNA (rDNA) regions (37). Approximately 10% of rDNA repeats were estimated to be cleaved (~30 to 50 DSB sites) (49), which cluster around the nucleoli and allow cytological detection of protein recruitment and modifications at damage sites (50). Cell cycle-specific recruitment of cohesin to I-PpoI cut sites was confirmed by colocalization with Rad51, which clusters to damage sites in an S/$G_2$-specific manner (51) (Fig. 1B and C). Thus, significant cohesin accumulation appears to be restricted to S/$G_2$ phase at both laser-induced and endonuclease-induced DSB sites.

**NIPBL requires cohesin for damage site targeting.** In order to understand the mechanism of cohesin loading at damage sites, we examined the involvement of the cohesin loading factor NIPBL. Using antibody specific for NIPBL (Fig. 2D), we found that NIPBL recruitment to damage sites is also restricted to S/$G_2$ phase (Fig. 2A and B). NIPBL accumulates at damage sites with kinetics similar to cohesin (see Fig. S2B in the supplemental material). As in yeast (21, 22), NIPBL is required for cohesin accumulation at damage sites in human cells, further supporting the idea that the observed clustering of cohesin reflects physiological loading of the complex (Fig. 2C). Interestingly, however, unlike cohesin-independent genome-wide loading of NIPBL in telophase (17, 52), NIPBL recruitment to damage sites requires cohesin (Fig. 2C). Depletion of Rad21 did not affect the level of NIPBL and vice versa (Fig. 2E). Taken together, the results indicate that NIPBL and cohesin require each other for S/$G_2$-specific damage site accumulation in human cells and suggest that the mechanism of their damage site loading is distinct from that for their genome-wide loading in telophase.

**Individual cohesin subunit depletion differentially affects other subunits' stability and nuclear localization.** We attempted to identify which cohesin subunit may be responsible for directing cohesin recruitment to damage sites. For example, for condensin I, another SMC complex, we found that the chromosome-targeting domain in the hCAP-D2 subunit possesses damage site targeting activity (36). Thus, we first determined the effect of depletion of one cohesin subunit on the recruitment of other subunits in the complex. The total hSMC1 protein level is largely unaffected by depletion of other subunits, whereas the Rad21 protein level is

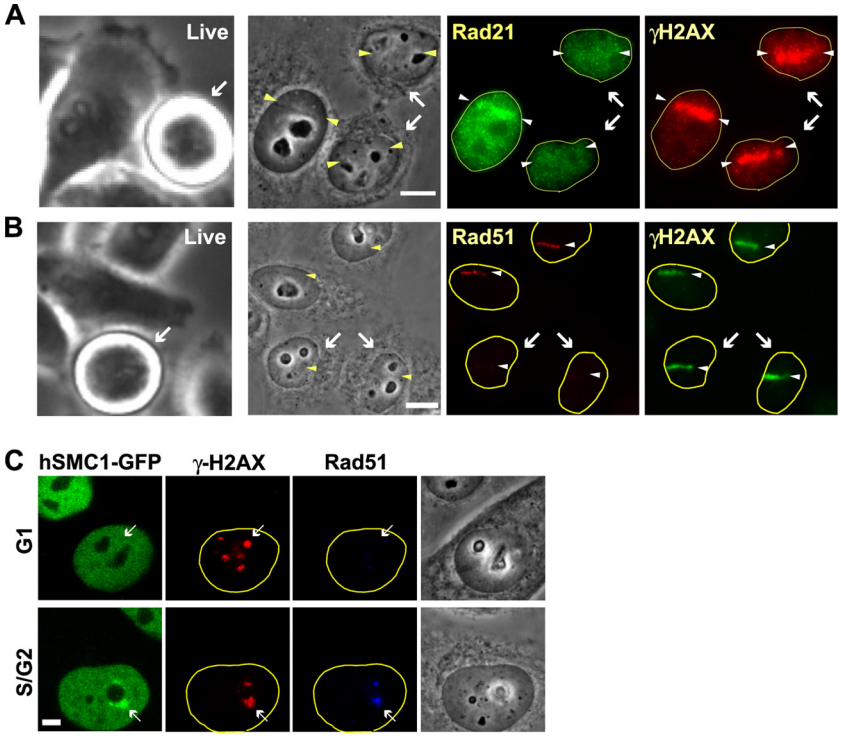


**FIG 1** S/$G_2$-specific recruitment of cohesin to sites of DSB damage induced by both laser microirradiation and I-PpoI endonuclease cleavage. (A) The endogenous Rad21 is recruited to laser-induced damage sites in S/$G_2$ but not $G_1$ cells. The left panel is the live image identifying the cell in metaphase. After 3 h, the same metaphase cell has divided into two daughter cells in $G_1$ (indicated by arrows). These newly divided cells and the larger adjacent cell that remained in interphase were damaged with the laser and, after 1 h, they were fixed and stained with antibodies specific for Rad21 and γH2AX. Scale bar, 10 μm. (B) Rad51 recruitment is also restricted to S/$G_2$ cells. Similar experiments were performed as in panel A, and cells were stained with antibodies specific for Rad51 and γH2AX. Scale bar, 10 μm. (C) hSMC1-GFP is recruited to DSBs induced by I-PpoI in an S/$G_2$-specific manner. The stable cell line expressing hSMC1-GFP was transfected with ER-I-PpoI, which was induced to relocalize to the nucleus for 10 h by 4-OHT. Cells were fixed and costained with antibodies specific for γH2AX (red) and Rad51 (blue). I-PpoI-induced DSB sites are indicated by arrows. Scale bar, 5 μm.

highly sensitive to depletion of other subunits (Fig. 3A). Interestingly, while depletion of hSMC1 and Rad21 caused partial decreases of SA1 and SA2 protein levels, SA1 depletion appeared to result in an increase of SA2 and vice versa, respectively, suggesting a compensatory regulation of SA1 and SA2 protein expression.

Immunostaining largely reflected the Western analyses except that hSMC1 seems to be absent in the nucleus following Rad21 depletion (Fig. 3B). Methanol fixation without detergent extraction revealed that the major population of hSMC1 is retained in the cytoplasm in the absence of Rad21 (Fig. 3B, methanol [MeOH] fix). Consistently, double depletion of SA1 and SA2, which significantly decreases Rad21, also resulted in cytoplasmic retention of hSMC1 (Fig. 3B). Thus, the results indicate that hSMC1 requires Rad21 for nuclear localization. In contrast, hSMC1 and Rad21 depletion only partially decreases the amount of SA2, and the residual SA2 nevertheless localizes to the nucleus, indicating that SA2 nuclear localization is independent of other cohesin subunits (Fig. 3B). The results reveal that individual cohesin subunits have different sensitivities with regard to stability and/or localization to the depletion of other subunits.

**Holo-cohesin-SA2 accumulates at damage sites.** Although double depletion of SA1 and SA2 abolished hSMC1 and Rad21 signals in the nucleus, SA2 depletion alone only partially decreased the hSMC1 and Rad21 levels without significantly affecting their localization pattern in the nucleus, likely because cohesin-SA1 is intact (Fig. 3B) (9, 10). The clustering of hSMC1 to damage sites, however, is completely abolished by SA2 depletion (Fig. 4). Similarly, depletion of either hSMC1 or Rad21 abolished the recruitment of SA2 to the damage site (Fig. 4), even though some SA2 still remains in the nucleus (Fig. 3B). This indicates that the intact cohesin complex is required for stable association with DNA damage sites and further raises the possibility that cohesin-SA1 is not present at DNA lesions.

Using antibodies specific for SA1 and SA2, we found significant accumulation of endogenous SA2 at the damage site but not SA1 (Fig. 5A). This preferential clustering of SA2 was also observed at the I-PpoI-induced DSB sites (Fig. 5B; see Fig. S3 in the supplemental material). Consistent with this, whereas depletion of SA2 abolished hSMC1-GFP clustering at the damage sites, depletion of SA1 had no effect (Fig. 5C). Similarly, depletion of SA2 but not SA1 abolished NIPBL accumulation at damage sites (Fig. 5D). The results indicate that cohesin-SA2, but not cohesin-SA1, is the major cohesin complex that accumulates at DNA lesions.

To address the mechanism of differential recruitment, we investigated whether the two cohesin complexes interact differently with the Mre11 complex. We previously showed that the Mre11 complex interacts with cohesin in an interphase-specific and DNA-independent manner and that Mre11-Rad50 (but not Nbs1) is required for cohesin recruitment to damage sites (19). We performed similar co-IP experiments for both endogenous SA1 and SA2, in addition to GFP-SA1 and GFP-SA2 stable cell lines with or without DNA damage. No significant difference was

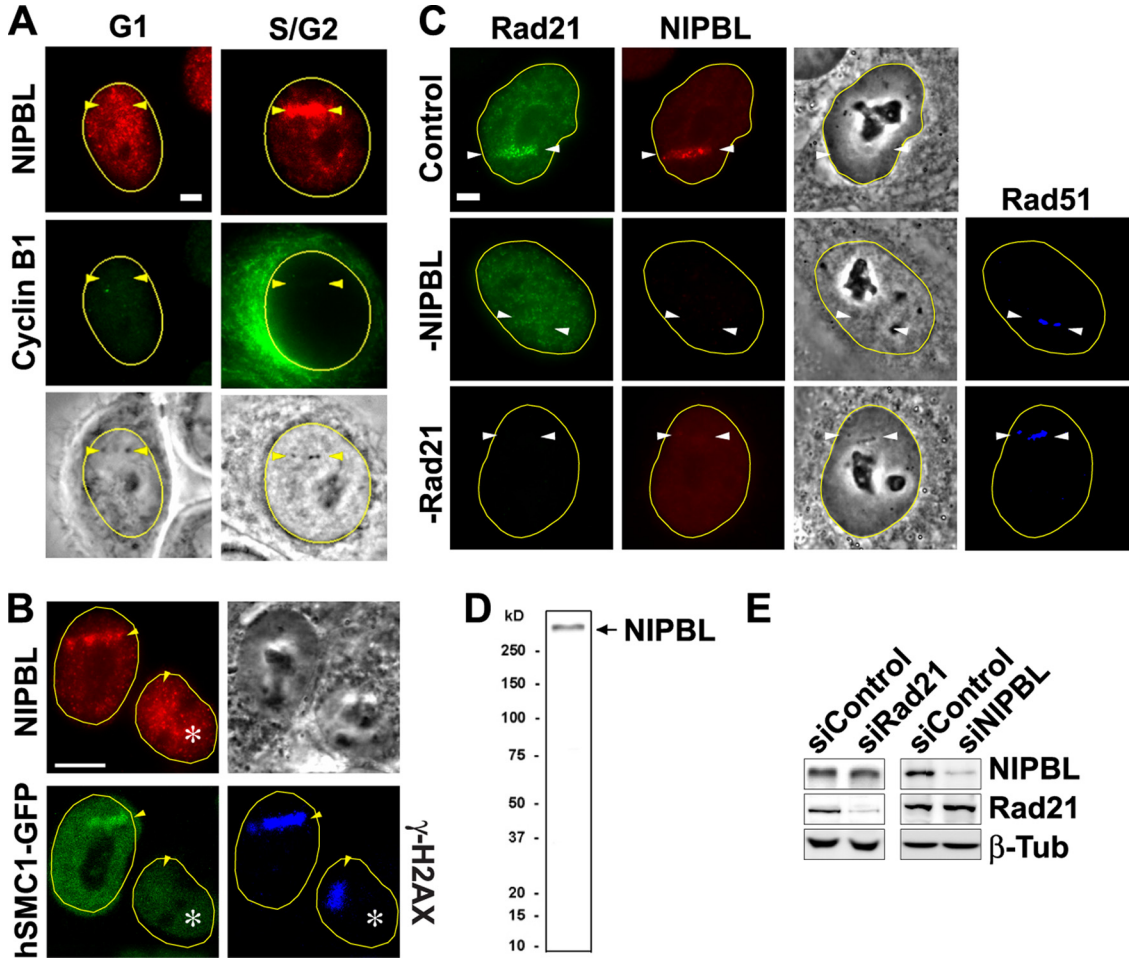


**FIG 2** S/$G_2$-specific corecruitment of the cohesin loading factor NIPBL and cohesin. (A) Immunofluorescent staining of HeLa cells in $G_1$ and S/$G_2$ with anti-NIPBL antibody (red) and anti-cyclin B1 antibody (green). Scale bar, 5 μm. (B) Similar analysis as in panel A of laser damage induced in $G_1$ (indicated by an asterisk) and S/$G_2$ cells stably expressing hSMC1-GFP costained with NIPBL (red) and γH2AX (blue). Scale bar, 10 μm. (C) Immunofluorescent staining of control, NIPBL, or Rad21 siRNA-treated cells with the indicated antibodies. Rad51 (blue) is used as the S/$G_2$-specific damage marker. Scale bar, 5 μm. (D) Western analysis of HeLa nuclear extracts probed with anti-NIPBL antibody. (E) Western analysis of control, Rad21, and NIPBL siRNA-treated cells. Extracts were probed with antibodies specific for the indicated proteins.

observed between the Mre11 complex interaction with cohesin-SA1 or with cohesin-SA2 (see Fig. S4A; and B in the supplemental material). Thus, preferential association of cohesin-SA2 with DSB sites is not due to differential interaction with the Mre11 complex. Furthermore, we confirmed that cohesin-SA1 and cohesin-SA2 do not interact with each other in either the presence or absence of damage (see Fig. S4B and C in the supplemental material). Thus, the two cohesin complexes remain as separate entities in the DNA damage response process.

**The C terminus of SA2 confers damage site targeting activity on SA1.** Although SA1 and SA2 are considered homologs, their functional domains have not been fully characterized. We generated stable cell lines expressing GFP-tagged full-length and deletion mutants of SA1 and SA2. The incorporation of the recombinant proteins into the cohesin complex was examined by *in vivo* co-IP using antibody specific for Rad21 that tethers the SA proteins to the SMC1-SMC3 heterodimer (53) (see Fig. S5 in the supplemental material). Rad21 efficiently coprecipitated the full-length SA1 and SA2 proteins, as well as the N-terminal and middle domain of SA1 (SA1NM) and SA2NM, both of which include the Irr1/STAG domains, whereas only weak interaction was observed with the N-terminal regions (SA1N and SA2N) that lack part of the Irr1 region (see Fig. S5). In contrast, no interaction was observed between the C-terminal regions of SA1 and SA2 (SA1C and SA2C) with Rad21. The results revealed that the conserved region containing the Irr1/STAG domain (>90% homology, shown in red) is important for cohesin complex formation (Fig. 6D).

The N- and C-terminal domains of SA1 and SA2 share only 30 to 50% homology, likely contributing to their functional specificities. Consistent with their independent nuclear localization (Fig. 3B), SA1 and SA2 have their own NLSs, but in different domains (see Fig. S5A and D and Fig. S6 in the supplemental material) (54). SA1N localizes to the nucleus consistent with the presence of a unique putative bipartite NLS, which is not present in SA2N (Fig. 6B; see also Fig. S6A and B in the supplemental material). Interestingly, SA2N localizes to the cytoplasm despite its diffusible size, suggesting an active sequestration that prevents diffusion (see Fig. S5D in the supplemental material). SA2C contains three putative NLSs and is clearly in the nucleus (Fig. 6B; see Fig. S5D and S6C in the supplemental material). One of the three putative NLSs is

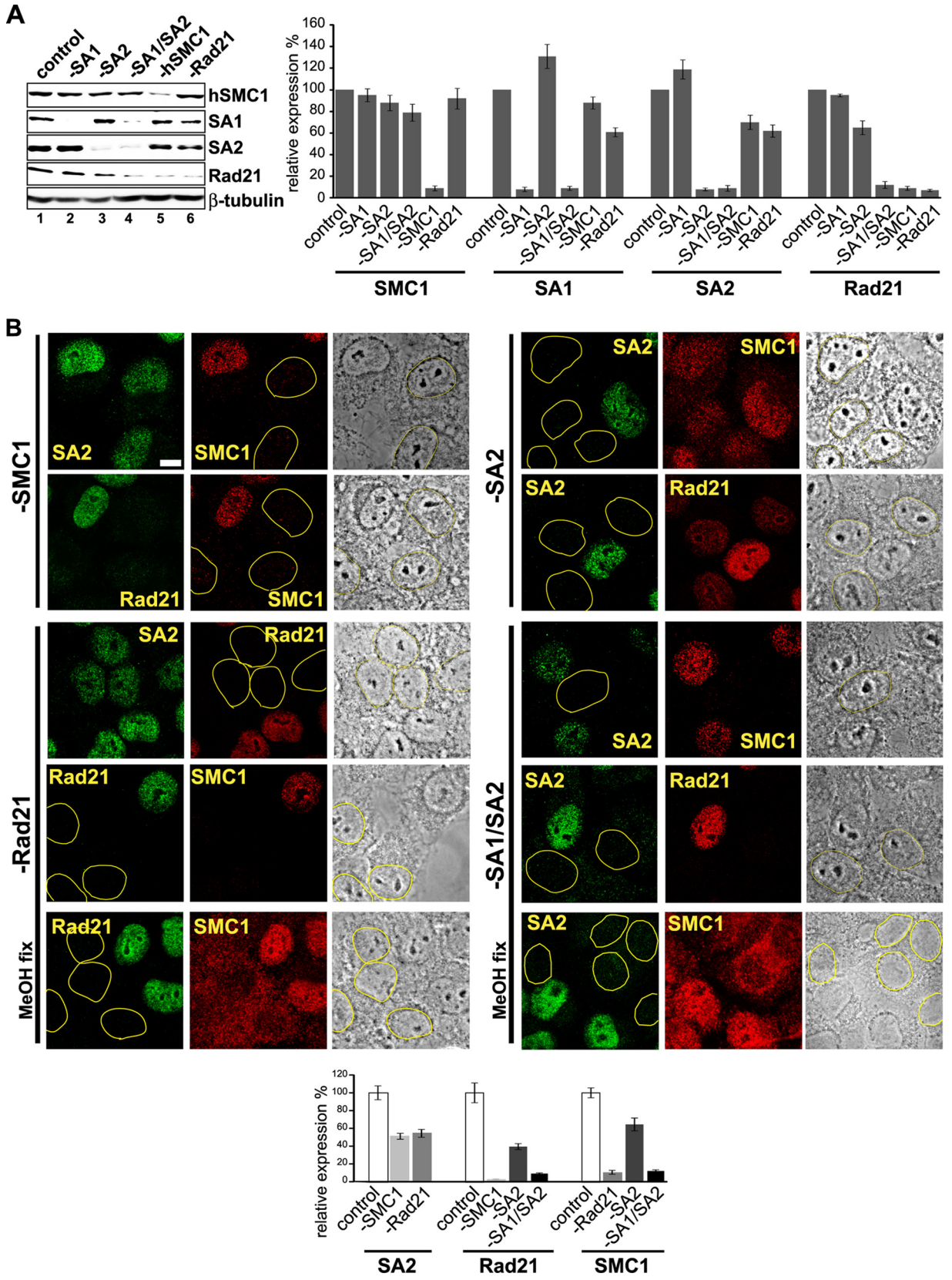


**FIG 3** Different effects of cohesin subunit depletion on other subunits. (A) Western blot analysis of cohesin subunit depletion. Proteins depleted by siRNAs are indicated at the top. Proteins detected by Western blotting are indicated on the right. β-Tubulin serves as a loading control. Quantification of the Western blot was done using the Quantity One quantification software (Bio-Rad). (B) Differential effects of cohesin subunit depletion on other subunits. siRNA-depleted proteins are indicated on the left. Proteins detected by immunofluorescent staining are indicated. For Rad21 and SA1/SA2 depletion, methanol-fixed cell staining without extraction is included (MeOH fix). Light microscope pictures are also shown. The nuclei of depleted cells are indicated by yellow lines. Scale bar, 10 μm. Quantification of fluorescent signals was done using Quantity One (Bio-Rad) and is shown at the bottom.

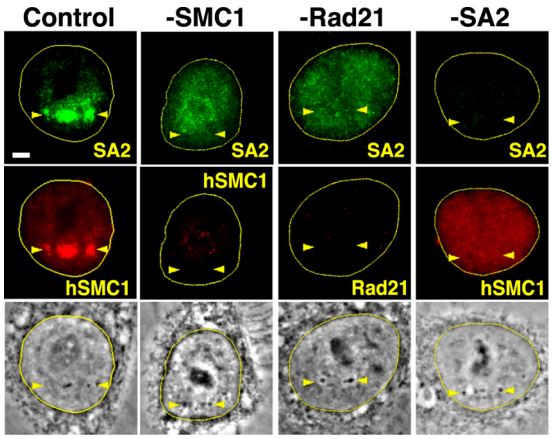


**FIG 4** The intact cohesin complex is required for stable association at DNA damage sites. HeLa cells were treated with control siRNA or siRNAs against hSMC1, Rad21, or SA2 and synchronized to S/$G_2$. At 1 h after damage induction, cells were fixed and stained with indicated antibodies. Scale bar, 5 μm.

conserved in SA1C, but the SA1C localization is not restricted to the nucleus and diffuses throughout the cytoplasm (see Fig. S5D in the supplemental material). Consistent with this, alanine substitution in this apparently conserved putative NLS (NLS3; "12X") had no significant effect on the nuclear localization of SA2C, suggesting that it is not functionally significant (see Fig. S5E and S6D in the supplemental material). In contrast, mutations of the second putative NLS (NLS2; "1X3"), which is missing in SA1, or the first NLS (NLS1; "X23"), which is only partially conserved in SA1, is sufficient to abolish the nuclear localization activity of SA2C (see Fig. S5E and S6D in the supplemental material). A recent study also identified functional NLSs in SA1N and SA2C although, unlike our results, NLS3 was shown to be sufficient to retain SA2 in the nucleus. The reason for this discrepancy is currently unclear (54).

Having defined the domains important for cohesin complex formation and nuclear localization, we next tested the damage site targeting of GFP-tagged SA1/SA2 chimeric mutants in stable lines. GFP-SA2 clusters to damage sites in an S/$G_2$-specific and Rad21-dependent manner, indicating that GFP-SA2 is recruited to DSBs in S/$G_2$-phase cells as part of the cohesin complex (Fig. 6A and B). Similar to the endogenous SA1, GFP-SA1 failed to accumulate at the damage sites (Fig. 6B). Time course measurement of the GFP signals in live cells confirmed the significant accumulation of GFP-SA2 at damage sites, which peaks at ~1.5 h and is detectable even after 8 h after damage induction (Fig. 6C). Although GFP-SA1 initially accumulates at damage sites with similar kinetics, the amount is much smaller and the signal peaks at an earlier time point, failing to further accumulate and stably associate with damage sites (Fig. 6C). The mutants lacking either SA1N or SA2C cannot localize to the nucleus (Fig. 6D; see Fig. S5D in the supplemental material) and thus were not tested for damage recruitment. Chimeric GFP-SA1NSA2MC and GFP-SA1NMSA2C not only localized to the nucleus but also clustered to the damage sites (Fig. 6B and D). GFP-SA1NMSA2C accumulates at damage sites in a manner similar to that of GFP-SA2 (Fig. 6C). Deletion of the last 62 aa in the C terminus eliminating NLS3 (GFP-SA2ΔNLS3) had no effect on nuclear localization of the full-length SA2 or its damage site targeting (Fig. 6B and D). SA2C alone, which goes to the nucleus but cannot be incorporated into the cohesin complex (Fig. 6E; see Fig. S5C in the supplemental material), failed to localize to the damage sites, an observation consistent with the requirement for holocomplex formation for damage site association (Fig. 4 and 6B). Taken together, replacing SA1C with SA2C is sufficient to confer damage site targeting activity on SA1, indicating the critical functional differences of the C termini of SA1 and SA2 (Fig. 6D).

**Cohesin-SA2 is preferentially involved in sister chromatid HR repair and affects repair pathway choice.** The important implication of the selective recruitment of cohesin-SA2 is that cohesin-SA2 may be the complex that is selectively involved in DSB damage response and repair. To address whether cohesin-SA2 is the primary cohesin complex involved in the actual repair of DSBs, SA1 and SA2 were individually depleted in synchronized cells, and the frequency of sister chromatid exchange (SCE) was assessed following DNA damage induced in S/$G_2$ phase. The SCE assay detects reciprocal exchange of sister chromatids following DSB damage in metaphase chromosome spreads and is used to measure the efficiency of HR repair specifically between sister chromatids (41, 44, 55). Depletion of Rad21, a subunit common to both cohesin-SA1 and cohesin-SA2, clearly decreased SCE as expected (Fig. 7A). Importantly, depletion of SA2 alone also compromised SCE, while this was not the case for SA1-only depletion. Similar results were obtained with additional lentivirus-transduced short hairpin RNAs (shRNAs) against SA1 and SA2 (data not shown). Mitotic indices were comparable in synchronized control and SA1- and SA2-depleted cells, and both proteins were depleted equally efficiently in metaphase cells without a prominent cohesion defect as previously described (40), indicating that the result is not due to the different effects of SA1 and SA2 depletion on cell cycle progression and/or selection of undepleted cells in mitosis (see Fig. S7 in the supplemental material).

It was shown that depletion of Rad21 enhances NHEJ repair, most likely due to the blockade of sister chromatid HR causing a shift of repair pathway choice (20). Consistent with this, we found that depletion of Rad21 and SA2 but not SA1 causes an increase of DNA end joining (Fig. 7B). There is no significant difference in the H2AX phosphorylation level in SA2-depleted cells compared to SA1-depleted or control siRNA-treated cells following irradiation (see Fig. S8 in the supplemental material), further suggesting that the removal of cohesin from damage sites does not lead to an overall decrease in DSB repair but rather affects the pathway choice of DSB repair. Taken together, cohesin-SA2, the primary cohesin recruited to DNA damage sites, specifically facilitates sister chromatid HR repair and antagonizes NHEJ repair of DSBs.

**Both cohesin-SA1 and cohesin-SA2 function in the intra-S checkpoint.** Cohesin also functions in the checkpoint response to promote cell survival following DNA damage. Cohesin was shown to be involved in the $G_2$/M checkpoint (26). Under our conditions, however, there was no apparent difference in the inhibition of mitotic entry at 4, 6, and 8 h after DNA damage in $G_2$ phase after control, SA1, or SA2 depletion, which were all equally alleviated by caffeine treatment that inhibits ATM/ATR kinases (Fig. 7C).

We found that phosphorylation of hSMC1, which is required for the intra-S checkpoint (25, 27), is comparable in the cohesin-SA1 and cohesin-SA2 complexes (Fig. 7D). Consistent with this,

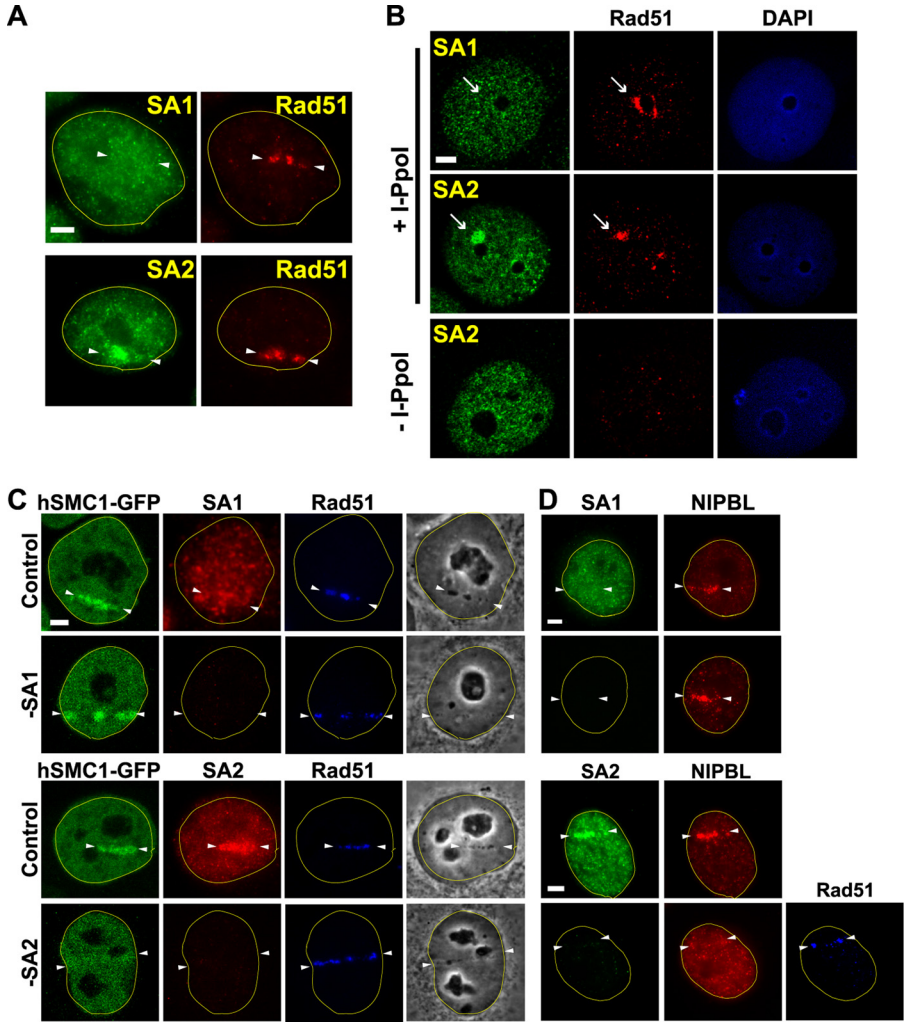


**FIG 5** Selective recruitment of cohesin-SA2 to damage sites. (A) Recruitment of SA2 but not SA1 to laser-induced damage sites. Laser damage was induced in S/$G_2$-phase cells and stained with indicated antibodies. Scale bar, 5 μm. (B) Accumulation of SA2 but not SA1 at I-PpoI-induced DSB sites. The bottom panels show the S/$G_2$ cell in the absence of I-PpoI. Rad51 and DAPI staining of DNA are also shown. Scale bar, 5 μm. (C) Effect of SA1 or SA2 depletion on hSMC1-GFP localization at laser-induced damage sites. HeLa cells stably expressing hSMC1-GFP were transfected with control siRNA or siRNA specific for SA1 or SA2 and synchronized with double thymidine block. Laser microirradiation was performed at 5 h after the second thymidine release. At 1 h after damage induction, hSMC1-GFP was detected in live cells, followed by fixation and immunostaining of SA1 or SA2 and Rad51. Scale bar, 5 μm. (D) Effect of SA1 or SA2 depletion on NIPBL localization at laser-induced damage sites. Cells were siRNA-depleted and synchronized as in panel C. Cells were fixed at 1 h after damage induction and stained with the indicated antibodies. Scale bar, 5 μm.

depletion of either SA1 or SA2 resulted in an increase of radioresistant DNA synthesis (RDS), a hallmark of an intra-S checkpoint defect (25, 27, 28) (Fig. 7E). Thus, cohesin-SA1 and cohesin-SA2 are both involved in the intra-S checkpoint, indicating that cytologically detectable damage site accumulation is not required for this function. Consequently, depletion of SA1 increased DNA damage sensitivity, indicating that cohesin-SA1 also plays an important role in the DNA damage response (Fig. 7F). Double depletion of SA1 and SA2 increased damage sensitivity to a level similar to the depletion of Rad21, further indicating that cohesin-SA1 and cohesin-SA2 both contribute to cell survival after DNA damage (Fig. 7F). Taken together, our results reveal the separation of the DSB repair and checkpoint functions of cohesin; the former mediated primarily by cohesin-SA2 that accumulates at damage sites, and the latter mediated primarily by both cohesin-SA1 and cohesin-SA2, most likely at their preexisting binding sites.

## DISCUSSION

Cohesin exhibits two functions in response to DNA damage: HR repair and a checkpoint response, but their relationship was unclear. In the present study, we found that only one of the two cohesin complexes, cohesin-SA2, significantly accumulates at damage sites and affects DSB repair by promoting sister chromatid HR and inhibiting NHEJ. This cohesin-SA2 clustering is S/$G_2$-restricted and requires NIPBL. However, unlike genome-wide loading in telophase, NIPBL recruitment to damage sites is also restricted to S/$G_2$ phase and is reciprocally dependent on cohesin-SA2. Although genome-wide sister chromatid cohesion in general was thought to contribute to postreplicative repair (56), our results indicate that the repair activity is specifically associated with cohesin accumulated at damage sites. In contrast to the predominant role of cohesin-SA2 in DSB repair, we found that depletion

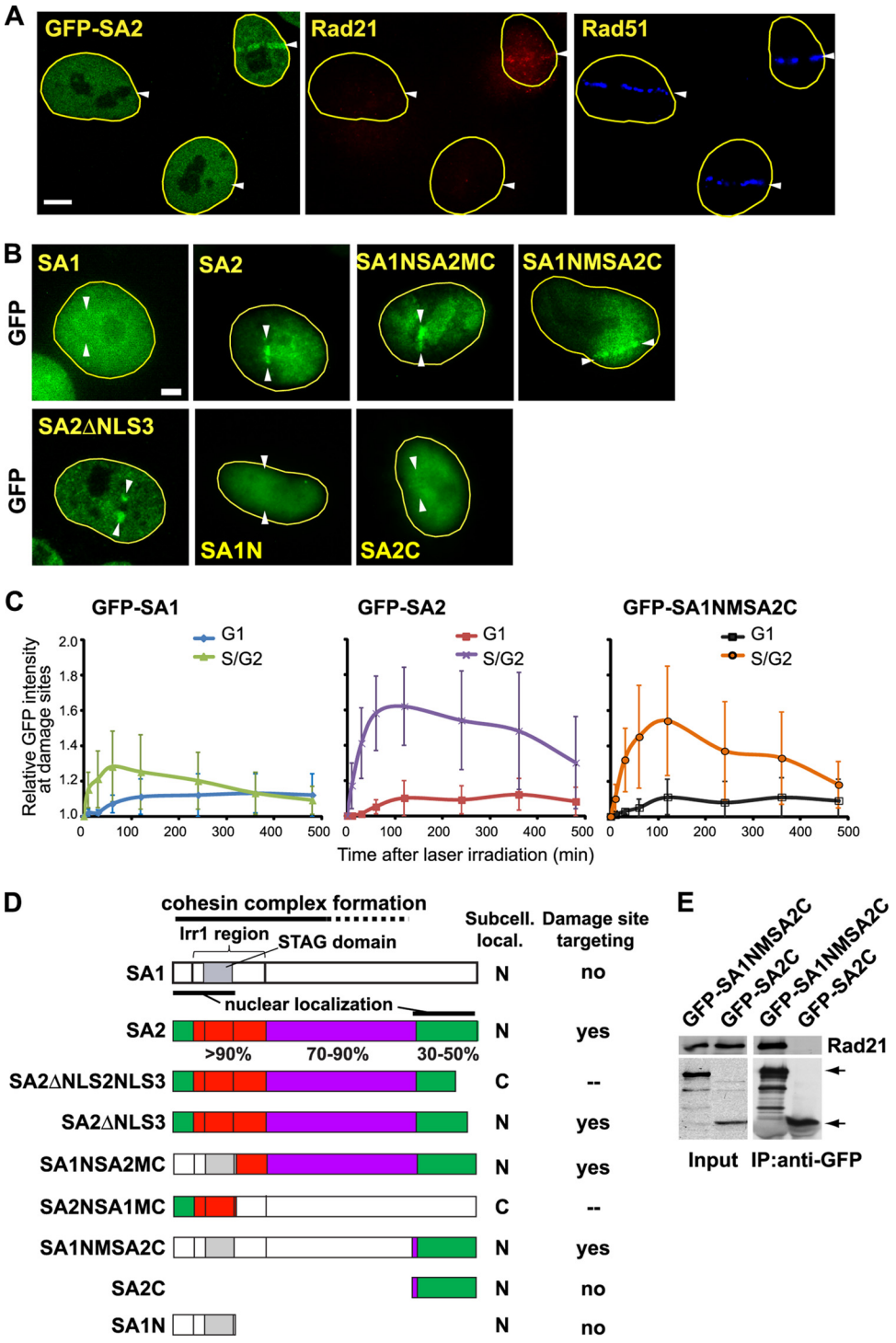


**FIG 6** SA2C confers damage site targeting activity on SA1. (A) GFP-SA2 localization at laser-induced damage sites in S/$G_2$ cells. A stable cell line expressing GFP-SA2 was treated with siRNA specific for Rad21 and was synchronized in S/$G_2$ for laser damage. GFP-SA2 was detected in live cells at 1 h after laser damage followed by cell fixation and staining with antibodies specific for Rad21 (red) and Rad51 (blue). Scale bar, 10 μm. (B) Stable HeLa cell lines expressing GFP-SA1, GFP-SA2, and various mutants as indicated were damaged, and the recruitment of the GFP fusion proteins was analyzed. Scale bar, 5 μm. (C) $G_1$- and S/$G_2$-phase cells expressing GFP-SA1, GFP-SA2, or GFP-SA1NMSA2C were damaged with 780-nm laser microirradiation, and accumulation of the GFP signal at the damage sites was measured at the indicated time in live cells. Relative GFP signals were calculated using GFP signal at the same area before damage induction in each cell as "1". (D) Summary of SA1 and SA2 mutants tested for damage site recruitment. The schematic diagrams of SA1 and SA2 deletion and chimeric mutants are shown. The homology between SA2 and SA1 is indicated by different colors. The conserved Irr1 region that contains the STAG domain, domains with the nuclear localization activity, and the Rad21 interaction (cohesin complex formation) domains are indicated. Nuclear (N) or cytoplasmic (C) localization and damage site targeting results ("yes," "no," or "–" [not tested]) of mutants are summarized. (E) Co-IP of GFP-SA1NMSA2C and GFP-SA2C using anti-GFP antibody. Precipitated materials were probed with anti-Rad21 and anti-GFP antibodies as indicated. Arrows indicate the GFP mutants.

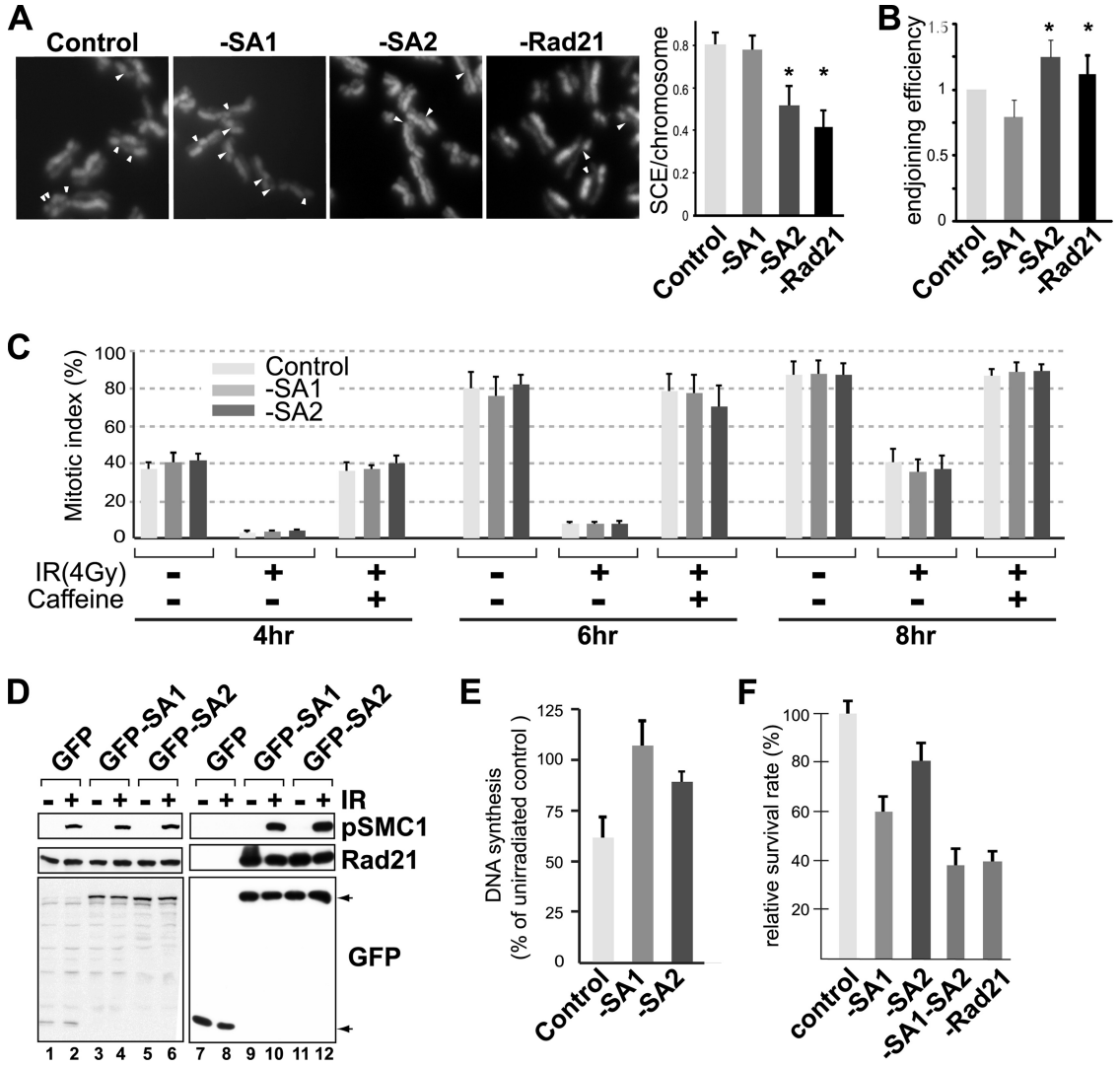


**FIG 7** Effects of SA1 and SA2 depletion on DNA damage response and repair. (A) The effect of SA1, SA2, or Rad21 depletion on sister chromatid HR repair. The SCE assay (see Materials and Methods) was performed using control, SA1, SA2, or Rad21 siRNA-treated cells. Depletion of the common subunit Rad21 was used for comparison. Example images of metaphase chromosome spreads and quantification of SCE are shown. Histogram data represent the means ± the standard errors of the mean (SEM) of 200 chromosomes from three separate experiments (*, $P < 0.03$ compared to the control). (B) The effect of SA1 and SA2 depletion on NHEJ repair. The end-joining efficiencies (see Materials and Methods) of SA1- and SA2-depleted cells were normalized to that of the control siRNA-treated cells in each experiment. Histogram data represent the means ± the SEM of $6 \times 10^5$ cells from three separate experiments (*, $P < 0.03$ compared to the control). (C) Effect of SA1 and SA2 depletion on the $G_2$/M checkpoint. siRNA-treated cells were synchronized by double-thymidine block and allowed to progress into $G_2$ phase and then were irradiated (4 Gy). The $G_2$ phase was confirmed by FACS analysis of DNA content (4N) and microscope analysis (not in mitosis) (data not shown). Mitotic indices were determined at 4, 6, and 8 h postirradiation with or without caffeine treatment as indicated. (D) Co-IP Western analysis of phosphorylation of hSMC1 (pSMC1) associated with GFP-SA1 and GFP-SA2. Nuclear extracts of stable cell lines expressing GFP only, GFP-SA1, or GFP-SA2 with or without damage (10 Gy IR) as indicated at the top were coprecipitated with anti-GFP antibody and probed with antibodies specific for pSMC1 and Rad21. Lanes 1 to 6, input; lanes 7 to 12, anti-GFP co-IP. The beads were probed with anti-GFP antibody to show comparable amounts of precipitated GFP fusion proteins. (E) RDS assay of SA1- and SA2-depleted cells. siRNA-treated cells were differentially labeled with $^{14}C$ and $^{3}H$ before and after 10 Gy IR (see Materials and Methods). The data were normalized against undamaged cells treated with the same siRNA. The data represent the means ± the SEM of three separate experiments (*, $P < 0.05$ compared to the control). (F) Cell survival assay of IR-damaged cells. Synchronized cells were irradiated with 5 Gy IR at S/$G_2$, and colonies were counted 2 weeks later. The data represent the means ± the SEM of three separate experiments (*, $P < 0.01$ compared to the control).

of either cohesin-SA2 or cohesin-SA1 compromised the intra-S damage checkpoint response and cell survival after damage. We conclude that the DSB repair and checkpoint functions of cohesin are separable, and cytologically visible cohesin accumulation at damage sites is not necessary for checkpoint function (Fig. 8).

**Cell cycle-specific cohesin-SA2 accumulation at damage sites.** Our study unequivocally demonstrated that cohesins cluster at DSB lesions introduced by either laser or endonuclease systems and is cell cycle specific, as indicated by Rad51 staining. In a recent study by Caron et al., a small fold increase in Rad21 accumulation was observed at endonuclease AsiSI cut sites, which were comparable in $G_1$ and $G_2$/M by ChIP analysis (48). The reason for this discrepancy is currently unclear. It may be due to the differences in the methods and timing to obtain $G_1$ cells. Although we examined

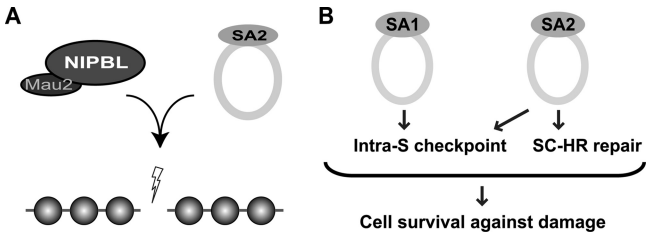


**FIG 8** Schematic model of the involvement of cohesin-SA1 and cohesin-SA2 in DNA damage response/repair. (A) Schematic diagram of S/$G_2$-specific corecruitment of NIPBL and cohesin-SA2 to the damage sites in an S/$G_2$-specific manner. The Mre11 complex and the NIPBL binding partner Mau2 are also shown. (B) Both unique and overlapping functions of the two complexes cooperatively protect genomic integrity and function from DNA damage.

early-$G_1$-phase cells during normal cell cycling, the cells were released from serum starvation for 10 h in Caron et al.'s study (48), which may include some cells in early S phase, where cohesin begins to accumulate at damage sites. Alternatively, as we also observed by fluorescence measurement, there is a small increase of cohesin binding at damage sites in the $G_1$ phase, which might have been detected by ChIP. However, no increase in ChIP signal in $G_2$ cells compared to $G_1$ (48) implies that ChIP may not be able to quantitatively detect further accumulation of cohesin at damage sites in S/$G_2$, possibly due to limitations associated with cross-linking and/or IP efficiency.

Similarly, ChIP using antibodies specific for SA1 and SA2 failed to reveal any difference between SA1 and SA2 binding at DSB sites in the study by Caron et al. (48). In our study, preferential accumulation of SA2 over SA1 at damage sites was confirmed with both specific antibodies and GFP-fusion constructs, as well as differential depletion effects on NIPBL and other cohesin subunits. Thus, ChIP-PCR does not reflect the cytologically detectable accumulation of cohesin at damage lesions. We also observed a transient accumulation of the GFP-SA1 signal at damage sites in S/$G_2$, although weaker than GFP-SA2 or the chimeric mutant, by fluorescence measurement. Thus, it is possible that chemical cross-linking artificially stabilizes this transient unstable recruitment of cohesin-SA1 for the ChIP analysis. In addition, since antibodies against SA1 and SA2 may have different ChIP efficiencies at damage sites, it may be difficult to compare the two ChIP signals. To further address this discrepancy and to circumvent the problem of comparing antibodies with different ChIP efficiencies, we performed Rad21 ChIP at I-PpoI sites in SA1- or SA2-depleted cells and observed that SA2 depletion affects damage-induced Rad21 binding enhancement more than SA1 depletion at damage sites but not at a distant undamaged locus (see Fig. S9 in the supplemental material). However, since there is a compensatory increase of SA2 in SA1-depleted cells and the Rad21 level appears to be decreased more in SA2-depleted cells (Fig. 3B), even these ChIP results may be skewed, and we must be cautious with their interpretation. Furthermore, since these ChIP analyses were performed in repair-proficient cells, it may be difficult to obtain clear results from a mixed population of cells with ongoing damage and repair at a given site, compared to the single cell analyses performed in the present study. Further work is needed to address the discrepancy between cytological and ChIP detection of cohesin binding at damage sites.

**Interdependent recruitment of cohesin-SA2 and NIPBL.** In yeast, cohesin requires Scc2 (the NIPBL homolog) for damage site recruitment (21, 22). We found that human cohesin also requires NIPBL for its damage site recruitment, further supporting the idea that the cytologically detectable clustering of cohesin at damage sites reflects physiological loading of the complex. This is also consistent with our finding that the intact cohesin complex is required for damage site association. Interestingly, however, NIPBL localization at damage sites is also cell cycle stage specific and is reciprocally dependent on cohesin in human cells. This is in contrast to genome-wide cell cycle-regulated NIPBL/cohesin loading in telophase, in which cohesin requires NIPBL, whereas NIPBL loading is independent of cohesin (17, 52). Thus, our results indicate that cohesin and NIPBL utilize a distinct mechanism for damage site loading and raise the possibility that the initial recruitment of cohesin and NIPBL to the damage site is dictated by cohesin. For example, we have shown that cohesin interacts with, and its recruitment is dependent upon, the Mre11-Rad50 complex in human cells (19), which may contribute to the initial recruitment of cohesin/NIPBL through protein-protein interaction(s). This, however, is not sufficient since the Mre11-Rad50 complex goes to damage sites throughout the cell cycle (19), and interacts with both cohesin-SA1 and cohesin-SA2 in a comparable fashion. It is conceivable that the presence of sister chromatids and/or an additional factor(s) (e.g., Wapl antagonists such as ESCO1/2 and sororin) contributes to the cell cycle-specific cohesin-SA2/NIPBL recruitment. Our finding that replacement of the C terminus of SA1 with that of SA2 confers damage site targeting activity provides the basis for future work to further dissect the underlying mechanism.

**Separation of the repair and checkpoint functions of cohesin.** Our results indicate that cohesin-SA2 that accumulates at damage sites is selectively involved in DNA repair, promoting sister chromatid HR and suppressing NHEJ. Although cohesin and Rad51 both accumulate at damage sites in an S/$G_2$-specific manner, cohesin depletion had no effect on Rad51 accumulation at both laser- and endonuclease-induced damage sites, indicating that the decreased sister chromatid HR is not due to the impairment of Rad51 recruitment to the damage sites.

In contrast to sister chromatid HR, the sister chromatid cohesion function is not required for checkpoint responses in human cells (26). In addition, we previously showed that S/$G_2$-specific cohesin clustering at damage sites is unaffected in A-T cells in which ATM is mutated and the intra-S checkpoint is compromised (19, 57), further supporting the notion that cohesin's recruitment to damage sites and its role in the intra-S checkpoint are separate. Exactly how cohesin is involved in the intra-S checkpoint response is not understood (18). Cohesin was shown to be involved in the ATM/Nbs1-dependent but not Chk2-Cdc25A-mediated intra-S checkpoint (25, 27, 28). Consistent with this, we did not see any significant effect on Chk2 phosphorylation in S phase by SA1 or SA2 depletion (see Fig. S10 in the supplemental material). Cohesin-SA1 participates in the intra-S checkpoint without significantly clustering at damage sites, raising the possibility that it functions in this checkpoint pathway at its preexisting binding sites in the genome. In fact, reinforcement of cohesin binding at preexisting binding sites, rather than redistribution to a new location, was observed by ChIP-seq analysis in response to irradiation (58). Importantly, this enhancement of cohesin binding requires SMC phosphorylation by ATM, which is critical for the intra-S checkpoint (58). Interestingly, the increase of cohesin binding at

AsiSI-cut sites detected by ChIP analysis (48) coincides with the preexisting cohesin binding sites, suggesting that the observed enhancement of cohesin binding may reflect the reinforcement of cohesin binding related to checkpoint signaling. In this case, it is reasonable that this enhanced cohesin binding was observed in both $G_1$ and $G_2$ phase of the cell cycle in a similar way and with both cohesin-SA1 and cohesin-SA2 (48), since SMC phosphorylation by ATM occurs throughout the cell cycle (26, 30) and both complexes are subject to ATM phosphorylation, as we demonstrated here. Taken together, it is possible that localized enhancement of cohesin binding (involving both cohesin-SA1 and cohesin-SA2) at its preexisting binding sites occurs throughout interphase as part of damage checkpoint signaling.

**Cooperativity of cohesin-SA1 and cohesin-SA2 in mammalian somatic cells.** Recent studies highlighted nonredundant roles of cohesin-SA1 and cohesin-SA2 in mammalian cells. The disruption of SA2 is associated with aneuploidy in a diverse range of human cancers, even in the presence of the intact SA1 gene (59), and SA1 knockout causes aneuploidy and certain types of cancers in mice even in the presence of SA2 (60). The loss of SA1 preferentially disrupts sister chromatid cohesion at telomeres, indicating the specialized role of cohesin-SA1 in telomere cohesion (11, 12, 60). Furthermore, evidence indicates that SA1 and SA2 have nonredundant functions in transcriptional regulation of certain genes (13). Thus, our study demonstrating the specialized role of cohesin-SA2 in DSB repair provides another dimension to the unique roles of cohesin-SA1 and cohesin-SA2 in the cell.

We found that SA proteins are largely stable and cluster in the nucleus in the absence of the other cohesin subunits, whereas their depletion affects Rad21's stability and thus compromises SMC1 nuclear localization. This apparent superordinate status of SA proteins in terms of protein stability and subcellular localization in relation to other cohesin subunits is consistent with the notion that SA1 and SA2 can dictate the functional specificity of each cohesin complex. Interestingly, however, a recent study showed that degron-mediated depletion of Scc3 (SA homolog) had no significant effect on the remainder of the cohesin complex's binding to DNA in yeast (61). Thus, the function of the SA proteins may have expanded during evolution. It is interesting to speculate that the appearance of two SA proteins was necessary to accommodate the increasing roles for cohesin in metazoan chromosome dynamics and regulation.

It should be noted, however, that cohesin-SA1 and cohesin-SA2 also have similar functions. For example, SA1 and SA2 colocalize at spindle poles, and their depletion exhibits a similar spindle assembly defect phenotype in human cells (40). Many cohesin binding sites identified by ChIP in the genome are bound by both complexes in human and mouse cells, suggestive of the shared functions (13, 46), which is consistent with the similar chromatin binding of the two complexes initially reported in humans and *Xenopus* (9). In the present study, we also found that both complexes are involved in the intra-S checkpoint and cell survival after damage. Although increased damage sensitivity of SA1- and SA2-depleted cells may be due to the defective intra-S checkpoint, gene expression changes caused by SA1 or SA2 depletion may also contribute to the phenotype. Taken together, there is cooperativity, in addition to a division of labor, between the two cohesin complexes in the cellular response to DNA damage.

**Conclusion.** Our findings reveal the unique ways in which the two human cohesin complexes participate in the DSB checkpoint response and repair. Our results demonstrate that both cooperativity and division of labor between the two cohesin complexes are critical for genome maintenance and cell survival.

## ACKNOWLEDGMENTS

We thank Hongtao Yu, Eva Lee, and Phang-Lang Chen for critical reading of the manuscript.

This study was supported in part by the National Institutes of Health (NIH) Laser Microbeam and Medical Program (RR01192), the Air Force Office of Scientific Research (FA9550-04-1-0101), and the Beckman Laser Institute, Inc., Foundation to M.W.B., and NIH CA100710 to K.Y.

## REFERENCES

1. **Ciccia A, Elledge SJ.** 2010. The DNA damage response: making it safe to play with knives. Mol. Cell **40:**179–204. http://dx.doi.org/10.1016/j.molcel.2010.09.019.
2. **Derheimer FA, Kastan MB.** 2010. Multiple roles of ATM in monitoring and maintaining DNA integrity. FEBS Lett. **584:**3675–3681. http://dx.doi.org/10.1016/j.febslet.2010.05.031.
3. **Shiloh Y.** 2003. ATM and related protein kinases: safeguarding genome integrity. Nat. Rev. Cancer **3:**155–168. http://dx.doi.org/10.1038/nrc1011.
4. **Carretero M, Remeseiro S, Losada A.** 2010. Cohesin ties up the genome. Curr. Opin. Cell Biol. **22:**781–787. http://dx.doi.org/10.1016/j.ceb.2010.07.004.
5. **Nasmyth K, Haering CH.** 2009. Cohesin: its roles and mechanisms. Annu. Rev. Genet. **43:**525–528. http://dx.doi.org/10.1146/annurev-genet-102108-134233.
6. **Onn I, Heidinger-Pauli JM, Guacci V, Unal E, Koshland DE.** 2008. Sister chromatid cohesion: a simple concept with a complex reality. Annu. Rev. Dev. Biol. **24:**105–129. http://dx.doi.org/10.1146/annurev.cellbio.24.110707.175350.
7. **Peters JM, Tedeschi A, Schmitz J.** 2008. The cohesin complex and its roles in chromosome biology. Genes Dev. **22:**3089–3114. http://dx.doi.org/10.1101/gad.1724308.
8. **Shintomi K, Hirano T.** 2010. Sister chromatid resolution: a cohesin releasing network and beyond. Chromosoma **119:**459–467. http://dx.doi.org/10.1007/s00412-010-0271-z.
9. **Losada A, Yokochi T, Kobayashi R, Hirano T.** 2000. Identification and characterization of SA/Scc3p subunits in the *Xenopus* and human cohesin complexes. J. Cell Biol. **150:**405–416. http://dx.doi.org/10.1083/jcb.150.3.405.
10. **Sumara I, Vorlaufer E, Gieffers C, Peters BH, Peters J-M.** 2000. Characterization of vertebrate cohesin complexes and their regulation in prophase. J. Cell Biol. **151:**749–761. http://dx.doi.org/10.1083/jcb.151.4.749.
11. **Canudas S, Houghtaling BR, Kim JY, Dynek JN, Chang WG, Smith S.** 2007. Protein requirements for sister telomere association in human cells. EMBO J. **26:**4867–4878. http://dx.doi.org/10.1038/sj.emboj.7601903.
12. **Canudas S, Smith S.** 2009. Differential regulation of telomere and centromere cohesion by the Scc3 homologues SA1 and SA2, respectively, in human cells. J. Cell Biol. **187:**165–173. http://dx.doi.org/10.1083/jcb.200903096.
13. **Remeseiro S, Cuadrado A, Gómez-López G, Pisano DG, Losada A.** 2012. A unique role of cohesin-SA1 in gene regulation and development. EMBO J. **31:**2090–2102. http://dx.doi.org/10.1038/emboj.2012.60.
14. **Hou F, Zou H.** 2005. Two human orthologues of EcoI/Ctf7 acetyltransferases are both required for proper sister-chromatid cohesion. Mol. Biol. Cell **16:**3908–3918. http://dx.doi.org/10.1091/mbc.E04-12-1063.
15. **Nishiyama T, Ladurner R, Schmitz J, Kreidl E, Schleiffer A, Bhaskara V, Bando M, Shirahige K, Hyman AA, Mechtler K, Peters JM.** 2010. Sororin mediates sister chromatid cohesion by antagonizing Wapl. Cell **143:**737–749. http://dx.doi.org/10.1016/j.cell.2010.10.031.
16. **Seitan VC, Banks P, Laval S, Majid NA, Dorsett D, Rana A, Smith J, Bateman A, Krpic S, Hostert A, Rollins RA, Erdjument-Bromage H, Tempst P, Benard CY, Hekimi S, Newbury SF, Strachan T.** 2006. Metazoan Scc4 homologs link sister chromatid cohesion to cell and axon migration guidance. PLoS Biol. **4:**1544–9173. http://dx.doi.org/10.1371/journal.pbio.0040242.
17. **Watrin E, Schleiffer A, Tanaka K, Eisenhaber F, Nasmyth K, Peters JM.** 2006. Human Scc4 is required for cohesin binding to chromatin, sister-chromatid cohesion, and mitotic progression. Curr. Biol. **16:**863–874. http://dx.doi.org/10.1016/j.cub.2006.03.049.

18. **Wu N, Yu H.** 2012. The Smc complexes in DNA damage response. Cell Biosci. **2:**5. http://dx.doi.org/10.1186/2045-3701-2-5.
19. **Kim J-S, Krasieva TB, LaMorte VJ, Taylor AMR, Yokomori K.** 2002. Specific recruitment of human cohesin to laser-induced DNA damage. J. Biol. Chem. **277:**45149–45153. http://dx.doi.org/10.1074/jbc.M209123200.
20. **Potts PR, Porteus MH, Yu H.** 2006. Human SMC5/6 complex promotes sister chromatid homologous recombination by recruiting the SMC1/3 cohesin complex to double-strand breaks. EMBO J. **25:**3377–3388. http://dx.doi.org/10.1038/sj.emboj.7601218.
21. **Ström L, Lindroos HB, Shirahige K, Sjögren C.** 2004. Postreplicative recruitment of cohesin to double-strand breaks is required for DNA repair. Mol. Cell **16:**1003–1015. http://dx.doi.org/10.1016/j.molcel.2004.11.026.
22. **Ünal E, Arbel-Eden A, Sattler U, Shroff R, Lichten M, Haber JE, Koshland D.** 2004. DNA damage response pathway uses histone modification to assemble a double-strand break-specific cohesin domain. Mol. Cell **16:**991–1002. http://dx.doi.org/10.1016/j.molcel.2004.11.027.
23. **Ström L, Karlsson C, Lindroos HB, Wedahl S, Katou Y, Shirahige K, Sjögren C.** 2007. Postreplicative formation of cohesion is required for repair and induced by a single DNA break. Science **317:**242–245. http://dx.doi.org/10.1126/science.1140649.
24. **Ünal E, Heidinger-Pauli JM, Koshland D.** 2007. DNA double-strand breaks trigger genome-wide sister-chromatid cohesion through EcoI (Ctf7). Science **317:**245–248. http://dx.doi.org/10.1126/science.1140637.
25. **Kim S-T, Xu B, Kastan MB.** 2002. Involvement of the cohesin protein, Smc1, in Atm-dependent and independent responses to DNA damage. Genes Dev. **16:**560–570. http://dx.doi.org/10.1101/gad.970602.
26. **Watrin E, Peters JM.** 2009. The cohesin complex is required for the DNA damage-induced $G_2$/M checkpoint in mammalian cells. EMBO J. **28:**2625–2635. http://dx.doi.org/10.1038/emboj.2009.202.
27. **Yazdi PT, Wang Y, Zhao S, Patel N, Lee EY-HP, Qin J.** 2002. SMC1 is a downstream effector in the ATM/NBS1 branch of the human S-phase checkpoint. Genes Dev. **16:**571–582. http://dx.doi.org/10.1101/gad.970702.
28. **Luo H, Li Y, Mu JJ, Zhang J, Tonaka T, Hamamori Y, Jung SY, Wang Y, Qin J.** 2008. Regulation of intra-S phase checkpoint by IR-dependent and IR-independent phosphorylation of SMC3. J. Biol. Chem. **283:**0021–9258. http://dx.doi.org/10.1074/jbc.M802299200.
29. **Sjögren C, Ström L.** 2010. S-phase and DNA damage activated establishment of sister chromatid cohesion: importance for DNA repair. Exp. Cell Res. **316:**1445–1453. http://dx.doi.org/10.1016/j.yexcr.2009.12.018.
30. **Kitagawa R, Bakkenist CJ, McKinnon PJ, Kastan MB.** 2004. Phosphorylation of SMC1 is a critical downstream event in the ATM–NBS1–BRCA1 pathway. Genes Dev. **18:**1423–1438. http://dx.doi.org/10.1101/gad.1200304.
31. **Jessberger R.** 2009. Cohesin's dual role in the DNA damage response: repair and checkpoint activation. EMBO J. **28:**2491–2493. http://dx.doi.org/10.1038/emboj.2009.217.
32. **Paschal CR, Bhalla N.** 2011. The cohesin complex: a platform for checkpoint activation and DNA repair? Curr. Biol. **21:**R649–R650. http://dx.doi.org/10.1016/j.cub.2011.07.039.
33. **Hou F, Chu CW, Kong X, Yokomori K, Zou H.** 2007. The acetyltransferase activity of San stabilizes the mitotic cohesin at the centromeres in a shugoshin-independent manner. J. Cell Biol. **177:**587–597. http://dx.doi.org/10.1083/jcb.200701043.
34. **Gregson HC, Schmiesing JA, Kim J-S, Kobayashi T, Zhou S, Yokomori K.** 2001. A potential role for human cohesin in mitotic spindle aster assembly. J. Biol. Chem. **276:**47575–47582. http://dx.doi.org/10.1074/jbc.M103364200.
35. **Kong X, Mohanty SK, Stephens J, Heale JT, Gomez-Godinez V, Shi LZ, Kim JS, Yokomori K, Berns MW.** 2009. Comparative analysis of different laser systems to study cellular responses to DNA damage in mammalian cells. Nucleic Acids Res. **37:**e68. http://dx.doi.org/10.1093/nar/gkp221.
36. **Kong X, Stephens J, Ball AR, Jr, Heale JT, Newkirk DA, Berns MW, Yokomori K.** 2011. Condensin I recruitment to base damage-enriched DNA lesions is modulated by PARP1. PLoS One **6:**e23548. http://dx.doi.org/10.1371/journal.pone.0023548.
37. **Berkovich E, Monnat RJ, Jr, Kastan MB.** 2008. Assessment of protein dynamics and DNA repair following generation of DNA double-strand breaks at defined genomic sites. Nat. Protoc. **3:**915–922. http://dx.doi.org/10.1038/nprot.2008.54.
38. **Ball J, Schmiesing ARJA, Zhou C, Gregson HC, Okada Y, Doi T, Yokomori K.** 2002. Identification of a chromosome targeting domain in the human condensin subunit CNAP1/hCAP-D2/Eg7. Mol. Cell. Biol. **22:**5769-5781. http://dx.doi.org/10.1128/MCB.22.16.5769-5781.2002.
39. **Heale JT, Ball JAR, Schmiesing JA, Kim JS, Kong X, Zhou S, Hudson D, Earnshaw WC, Yokomori K.** 2006. Condensin I interacts with the PARP-1-XRCC1 complex and functions in DNA single-stranded break repair. Mol. Cell **21:**837–848. http://dx.doi.org/10.1016/j.molcel.2006.01.036.
40. **Kong X, Ball ARJ, Sonoda E, Feng J, Takeda S, Fukagawa T, Yen TJ, Yokomori K.** 2009. Cohesin associates with spindle poles in a mitosis-specific manner and functions in spindle assembly in vertebrate cells. Mol. Biol. Cell **20:**1289–1301. http://dx.doi.org/10.1091/mbc.E08-04-0419.
41. **Sonoda E, Sasaki MS, Morrison C, Yamaguchi-Iwai Y, Takata M, Takeda S.** 1999. Sister chromatid exchanges are mediated by homologous recombination in vertebrate cells. Mol. Cell. Biol. **19:**5166–5169.
42. **Falck J, Forment JV, Coates J, Mistrik M, Lukas J, Bartek J, Jackson SP.** 2012. CDK targeting of NBS1 promotes DNA-end resection, replication restart and homologous recombination. EMBO Rep. **13:**561–568. http://dx.doi.org/10.1038/embor.2012.58.
43. **Zhao S, Renthal W, Lee EY.** 2002. Functional analysis of FHA and BRCT domains of NBS1 in chromatin association and DNA damage responses. Nucleic Acids Res. **30:**4815–4822. http://dx.doi.org/10.1093/nar/gkf612.
44. **Wu N, Kong X, Ji Z, Zeng W, Potts PR, Yokomori K, Yu H.** 2012. Scc1 sumoylation by Mms21 promotes sister chromatid recombination through counteracting Wapl. Genes Dev. **26:**1473–1485. http://dx.doi.org/10.1101/gad.193615.112.
45. **Zeng W, de Greef JC, Chen Y-Y, Chien R, Kong X, Gregson HC, Winokur ST, Pyle A, Robertson KD, Schmiesing JA, Kimonis VE, Balog JFRR, Ball JAR, Lock LF, Donovan PJ, van der Maarel S, Yokomori K.** 2009. Specific loss of histone H3 lysine 9 trimethylation and HP1γ/cohesin binding at D4Z4 repeats is associated with facioscapulohumeral dystrophy (FSHD). PLoS Genet. **5:**e1000559. http://dx.doi.org/10.1371/journal.pgen.1000559.
46. **Wendt KS, Yoshida K, Itoh T, Bando M, Koch B, Schirghuber E, Tsutsumi S, Nagae G, Ishihara K, Mishiro T, Yahata K, Imamoto F, Aburatani H, Nakao M, Imamoto N, Maeshima K, Shirahige K, Peters JM.** 2008. Cohesin mediates transcriptional insulation by CCCTC-binding factor. Nature **451:**796–801. http://dx.doi.org/10.1038/nature06634.
47. **Kim J-S, Krasieva TB, Kurumizaka H, Chen DJ, Taylor AM, Yokomori K.** 2005. Independent and sequential recruitment of NHEJ and HR factors to DNA damage sites in mammalian cells. J. Cell Biol. **170:**341–347. http://dx.doi.org/10.1083/jcb.200411083.
48. **Caron P, Aymard F, Iacovoni JS, Briois S, Canitrot Y, Bugler B, Massip L, Losada A, Legube G.** 2012. Cohesin protects genes against γH2AX Induced by DNA double-strand breaks. PLoS Genet. **8:**e1002460. http://dx.doi.org/10.1371/journal.pgen.1002460.
49. **Monnat J, Hackmann RJAFM, Cantrell MA.** 1999. Generation of highly site-specific DNA double-strand breaks in human cells by the homing endonucleases I-PpoI and I-CreI. Biochem. Biophys. Res. Commun. **255:**88–93. http://dx.doi.org/10.1006/bbrc.1999.0152.
50. **Oka Y, Suzuki K, Yamauchi M, Mitsutake N, Yamashita S.** 2011. Recruitment of the cohesin loading factor NIPBL to DNA double-strand breaks depends on MDC1, RNF168, and HP1γ in human cells. Biochem. Biophys. Res. Commun. **411:**762–767. http://dx.doi.org/10.1016/j.bbrc.2011.07.021.
51. **Tashiro S, Walter J, Shinohara A, Kamada N, Cremer T.** 2000. Rad51 accumulation at sites of DNA damage and in postreplicative chromatin. J. Cell Biol. **150:**283–291. http://dx.doi.org/10.1083/jcb.150.2.283.
52. **Bermudez VP, Farina A, Higashi TL, Du F, Tappin I, Takahashi TS, Hurwitz J.** 2012. In vitro loading of human cohesin on DNA by the human Scc2-Scc4 loader complex. Proc. Natl. Acad. Sci. U. S. A. **109:**9366–9371. http://dx.doi.org/10.1073/pnas.1206840109.
53. **Haering CH, Lowe J, Hochwagen A, Nasmyth K.** 2002. Molecular architecture of SMC proteins and the yeast cohesin complex. Mol. Cell **9:**773–788. http://dx.doi.org/10.1016/S1097-2765(02)00515-4.
54. **Tarnowski LJ, Kowalec P, Milewski M, Jurek M, Plochocka D, Fronk J, Kurlandzka A.** 2012. Nuclear import and export signals of human cohesins SA1/STAG1 and SA2/STAG2 expressed in *Saccharomyces cerevisiae*. PLoS One **7:**e38740. http://dx.doi.org/10.1371/journal.pone.0038740.
55. **West SC.** 2003. Molecular views of recombination proteins and their control. Nat. Rev. Mol. Cell. Biol. **4:**435–445. http://dx.doi.org/10.1038/nrm1127.
56. **Sjogren C, Nasmyth K.** 2001. Sister chromatid cohesion is required for postreplicative double-strand break repair in *Saccharomyces cerevisiae*. Curr. Biol. **11:**991–995. http://dx.doi.org/10.1016/S0960-9822(01)00271-8.
57. **Painter RB.** 1981. Radioresistant DNA synthesis: an intrinsic feature of ataxia telangiectasia. Mutat. Res.:183–190.
58. **Kim BJ, Li Y, Zhang J, Xi Y, Li Y, Yang T, Jung SY, Pan X, Chen R,**

**Li W, Wang Y, Qin J.** 2010. Genome-wide reinforcement of cohesin binding at preexisting cohesin sites in response to ionizing radiation in human cells. J. Biol. Chem. **285:**22784–22792. http://dx.doi.org/10.1074/jbc.M110.134577.

59. **Solomon DA, Kim T, Diaz-Martinez LA, Fair J, Elkahloun AG, Harris BT, Toretsky JA, Rosenberg SA, Shukla N, Ladanyi M, Samuels Y, James CD, Yu H, Kim JS, Waldman T.** 2011. Mutational inactivation of STAG2 causes aneuploidy in human cancer. Science **333:**1039–1043. http://dx.doi.org/10.1126/science.1203619.
60. **Remeseiro S, Cuadrado A, Carretero M, Martínez P, Drosopoulos WC, Cañamero M, Schildkraut CL, Blasco MA, Losada A.** 2012. Cohesin-SA1 deficiency drives aneuploidy and tumourigenesis in mice due to impaired replication of telomeres. EMBO J. **31:**2076–2089. http://dx.doi.org/10.1038/emboj.2012.11.
61. **Kulemzina I, Schumacher MR, Verma V, Reiter J, Metzler J, Failla AV, Lanz C, Sreedharan VT, Rätsch G, Ivanov D.** 2012. Cohesin rings devoid of Scc3 and Pds5 maintain their stable association with the DNA. PLoS Genet. **8:**e1002856. http://dx.doi.org/10.1371/journal.pgen.1002856.